PCCP

In-situ investigation of surface morphology evolution of bulk ceramic Y2Mo3O12 during crystal water releasing

SCHOLARONE™
Manuscripts

In-situ investigation of surface morphology evolution of bulk ceramic $Y_2Mo_3O_{12}$ during crystal water releasing

Y.G. Cheng,[a,b] X.S. Liu,[c] H.J. Chen,[d] M.J. Chao[a] and E.J. Liang[a*]

[a] *School of Physical Science & Engineering and Key Laboratory of Materials Physics of Ministry of Education of China, Zhengzhou University, Zhengzhou, 450051, China*

[b] *College of Science, Center of Analysis and Testing of Henan Institute of Engineering, Zhengzhou 451191, China*

[c] *Key Laboratory of Photovoltaic Materials of Henan Province and School of Physics and Electronics, Henan University, Kaifeng 475004, China*

[d] *Institute of Metallurgy, Henan Academy of Sciences, Zhengzhou, 450052, China*

Surface morphology evolution of bulk ceramic $Y_2Mo_3O_{12}$ during releasing process of crystal water is firstly traced in-situ by atomic force microscope. It is found that both the shape and size of individual grains and the integration morphology of sample exhibit dynamic changes with increasing temperature. We believe that the surface morphology evolution of the sample with increasing temperature are colsely correlated with the forces induced by contracting and expanding of the lattice during crystal water releasing in two different stages.

Keywords: Crystal water; Morphology evolution; AFM; Thermal expansion

PACS: 82.30.Rs Hydrogen bonding, hydrophilic effects

78.30.-j Infrared and Raman spectra

65.40.De Thermal expansion

---

[*] Corresponding author. Tel.: +86 371 67767838; fax: +86 371 67766629.
E-mail address: ejliang@zzu.edu.cn.

1. Introduction

Although some materials with negative thermal expansion (NTE) have been known for a long history, such as, the Invar alloy, the NTE phenomenon had not been appealed much attention untill the discovery of NTE in a large temperature range of α-ZrW$_2$O$_8$.[1] The discovery not only provokes scientific interests in NTE but also paves the way toward engineering thermal expansion property of materials,[2-6] which has potential applications in modern technologies, such as in solid state fuel cells, high precision instruments and spacecrafts, etc.

In recent years, an increament categories of materials with NTE based on different mechnisms were found. The largest category is the flexible framework structure such as tungstates or molybdates AM$_2$O$_8$ (A=Zr, Hf; M=W or Mo),[1,2] A$_2$M$_3$O$_{12}$ (A=transition metal or rare earth),[7-9] cyanides M(CN)$_2$ (M=Zn, Cd) and Ag$_3$[Co(CN)$_6$],[3] fluorides ScF$_3$,[4] phosphides NaZr$_2$P$_3$O$_{12}$,[10] vandates ZrV$_2$O$_7$,[11] and β-eucryptite,[12] etc. whose NTEs arise from the contribution of phonon anharmonicity[4-5] although the details of the mechanisms for them are still not clear. The second category is the anti-perovskite manganese nitrides Mn$_3$AN (A=Cu, Ge and Ni, etc.),[6,13] whose NTE is caused by magnetovolume effect accompanied by the transition from antiferromagnetism (AF) to paramagnetism (PM) phases. NTE was also found in perovskite ferroelectrics such as PbTiO$_3$ during ferroelectric-to-paraelectric phase transition.[5] Colossal NTE was also observed in perovskite LaCu$_3$Fe$_4$O$_{12}$ and BiNiO$_3$[14,15] by intersite charge transfer between the A-site (Cu or Bi) and B-site (Fe or Ni) ions, accompanied by PM-to-AF and metal-to-insulator isostructural phase transitions. Similar phenomena also appear during monoclinic-orthorhombic phase transition[8] or releasing and adsorbing of crystal water[16,17] in A$_2$M$_3$O$_{12}$ family. What would happen microscopically during the

giant expansion/contraction and do the microscopic changes have observable effect on the properties of materials? This is, however, essential from both the scientific and application point of view but has not been explored.

$Y_2Mo_3O_{12}$ is a model material in the $A_2M_3O_{12}$ family[18,19] and the influence of crystal water on the thermal expansion and phonon vibrations has been studied in detail.[16-17,19] The surface morphologies of powdered $Y_2Mo_3O_{12}$ with space groups of Pba2 and Pbcn were observed by Lind et al. using scanning electron microscopy (SEM) and the density of Pba2-$Y_2Mo_3O_{12}$ particles being higher than that of Pbcn-$Y_2Mo_3O_{12}$ were suggested.[20] Liu et al. presented SEM images of $Y_2Mo_3O_{12}$ ceramics consisting of grains and pores.[21] Those studies presented only 2D micromorphologies of $Y_2Mo_3O_{12}$ at   RT. To our knowledge, there is no report on the 3D morphology of $Y_2Mo_3O_{12}$ ceramics, especially on the evolution of surface morphology induced by releasing crystal water during temperature increasing.

In this paper, we use $Y_2Mo_3O_{12}$ ceramic body to pursue the surface morphology change during the releasing of crystal water on heating. 3D images of the sample at different temperatures were obtained with an atomic force microscopy (AFM). Colossal expansion or contraction occurs not only in $Y_2Mo_3O_{12}$ by crystal water releasing or admitting but also in a variety of materials during phase transitions as mentioned above. This work not only provides the effect of crystal water on the morphology of $Y_2Mo_3O_{12}$, but also opens the door towards in-situ pursuing the effect of phase transition related surface morphology evolution.

2. Experimental

2.1 Preparation of the powder and pellet samples ($Y_2Mo_3O_{12}$)

$Y_2Mo_3O_{12}$ was prepared by sol-gel method. Analytical reagents $Y(NO_3)_3 \cdot 9H_2O$ and $(NH_4)_6Mo_7O_{24} \cdot 4H_2O$ were used as raw materials. $C_6H_8O_7$ was used as

complexing agent. 30 ml (0.01 mol) aqueous solutions of $Y(NO_3)_3 \cdot 9H_2O$ was stirred with magnetic stirrer for 1 h at 323 K. Transparent sol was formed after adding $C_6H_8O_7$ (0.1 mol) to the above solution. $(NH_4)_6Mo_7O_{24} \cdot 4H_2O$ was then put into the sol to keep a molar ratio of Y:Mo=2:3. The sol was stirred rigorously at 353 K for 6 h and then heated in a blast oven at 408 K for 12 h. It was heated at 623 K for 3 h and at 973 K for another 3 h in a muffle furnace. The resultant powders were cooled naturally to room temperature (RT) and uniaxial cold pressed at 300 MPa into pellets followed by sintering at 1023 K for 4 h, thermal etching the pellets for AFM measurements.

2.2 Experimental techniques

Temperature-dependent X-ray diffraction (XRD) and Raman measurements were carried out in the temperature range of 293-423 K. High resolution transmission electron microscopy (HRTEM) was employed to investigation the microstructure and diffraction fringes. Simultaneous thermal analysis were done on a Netzsch STA (449F3) in the temperature range of 320-550 K with heating rates of 3 K/min. Morphology evolution of the grains at different temperature in 293-413 K was observed by AFM (Bruker Nano Inc., Dimension FastScan). The relative length change was measured with a dilatometer (LINSEIS DIL L75).

3. Results and discussion

3.1 Crystal structure

Fig. 1 shows the HRTEM image (insert: electron diffraction pattern) (a) and lattice diffraction fringes (b) of $Y_2Mo_3O_{12}$ powders. The HRTEM shows that $Y_2Mo_3O_{12}$ crystals synthesized with sol-gel method grow into nano-grains and aggregate to larger irregular-shaped clusters. As $Y_2Mo_3O_{12}$ is highly hygroscopic, it should be in a fully hydrated form of $Y_2Mo_3O_{12} \cdot 3H_2O$ at ambient atmosphere and

room temperature. The HRTEM image and diffraction fringes reflect the real status of the hydrated $Y_2Mo_3O_{12}\cdot3H_2O$ because the crystal waters are not physically adsorbed but chemically bonded.[22,24] The regular lattice diffraction fringes indicate no lattice distortion in the sample, i.e. the fully hydrated $Y_2Mo_3O_{12}\cdot3H_2O$ presents still periodic structure but the space group is different from the unhydrated $Y_2Mo_3O_{12}$ as reported by Lind et al.[20,23] It can be infered that the fully hydrated $Y_2Mo_3O_{12}\cdot3H_2O$ with space group Pba2 is energetically most favorable, and lattice distortion will occur during releasing of crystal water and enventally becomes unhydrated $Y_2Mo_3O_{12}$ with space group Pbcn.

3.2 Morphology evolution and thermal expansion with temperature

We select the temperatures at 293, 353, 373, 393 and 413 K to investigate the surface morphology evolution of $Y_2Mo_3O_{12}$ bulk ceramic with increasing temperature by AFM. Fig. 2 shows the 3D images of $Y_2Mo_3O_{12}$ ceramic at different temperatures observed by AFM. For the 3D image at 293 K, nano-grains pile together with few pores and some reunite into larger particles. When the temperature is increased from RT to 353 K, some grains at the valley grow up while those at higher brae and top contract obviously becomes more flaten. From 353 to 373 K, little morphological changes of the grains occur except that some grains become weakly wrinkled. As long as temperature is increased to 393 K, remarkable changes in morphology occur: most of grains became obviously wrinkled. And the wrinkles disappear at 413 K.

As can be seen below, the morphology changes in differen temperature ranges are related to the release of water species. From RT to 373 K, the surface physically adsorbed waters tend to be desorbed. The desorption of these water species will left some space among the grains and from the momentum conservation point of view, an impulse will be applied to the grains upon release of water species. Besides, the

surface energy around the edges is higher than that of a flaten surface and the surface water species tend to be adsorbed on higher enegy positions to make the system in a lowest energy in equalibrum. These factors are possibly the reasons for the relative shifts and rearrangements of the grains from RT to 373 K. From 373 to 393 K, the release of chemically bonded crystal waters accelerates and the grains are in a nonequalibrum state and experience an expansion and contraction during crystal water releasing. This is possibly the cause of the surface wrinkles.

In order to see the influence of crystal water releasing on the grains more clearly, we show in Fig. 3a-c the slices of the surface profiles of the central grain in different planes with increasing temperature. From RT to 373 K, the grain shows a progressive change in particle size. This process corresponds to the release of physically adsorbed water species. Remarkable changes in size and shape of the grain occur between 373 and 393 K as shown by Fig. 3a-c. We believe, this process is associated the release of crystal water chemically bonded in the microchannels of the building blocks.[17] It is obvious that the grain size change in the *YOZ* plane (Fig. 3b) is much more distinct than in the *XOZ* plane (Fig. 3a). In order to clearly present the differences in grain size/shape at different temperatures, we also draw the area of grain profile corresponding to the slices in different planes (*XOZ, YOZ* and 45° between *XOZ* and *YOZ* plane) with increasing temperature (Fig. 3d). It is clear that the abrupt contraction occurs between 373-393 K, and then the grain expands from 393 to 413 K.

The anisotropic changes in different planes may arise from the anisotropy in thermal expansion of $Y_2Mo_3O_{12}$ with crystal water. It was demostrated that the admission of crystal waters in $Y_2Mo_3O_{12}$ causes the *b*- and *c*- axises to contract more than the *a*-axis.[17] The change tendency of surface morphology in AFM images is

corresponding to the change of the relative length at variable temperatures in air with humidity of 55% RH (relative humidity) (Fig. 3e). However, in the vacuum with the pressure of -0.1 MPa, even at room temperature, there is no water to incorporate during the cooling process (Fig. 3f). The difference in temperature scope between the relative length change and AFM results could result from the difference in measurement methods. In the AFM measurements, the sample was kept at certain temperatures for certain time to capture the images while the relative length change was measured with continuous increase of temperature.

3.3 Proof of releasing crystal water

In order to repeat the change in surface size/shape of the sample, we have presented 3D images with increasing temperature from 293 to 413 K in another micro area in Fig. 4. Fig. 4 shows the fine observation near the grain in 2 μm×2 μm area. It confirms the similar effect of thermal contraction/expansion as given in Fig. 2. An integration evolution of the sample with increasing temperature is observed: the grains at the valley grow up and the top flattens, making the overall sample surface much flatter (see Fig. 2 and Fig. 4).

This indicates a dynamic shape variation with increasing temperature i.e. with the release of crystal water. We believe that the individual grain morphology change and integration evolution of the sample's morphology are closely correlated with the forces induced by contracting and expanding of the samples during crystal water releasing in the two stages.[16,19]

The process of the release and incorporation of crystal water is reversible in air with humidity of 55% RH, as revealed in Fig. 3e. With increasing temperature from 373 to 413 K, there appears the release process of crystal water for $Y_2Mo_3O_{12}$ in air under normal pressure. When the temperature decreases from 413 K to 333 K, the

process of incorporation of water takes place according to our previous investigation on temperature-dependent Raman spectra of $Y_2Mo_3O_{12}$[16] and the relative length change in air (Please see Fig. 3e). However, in the vacuum with the pressure of -0.1 MPa, even at room temperature, there is no water to incorporate during the cooling process (Fig. 3f), i.e. the thermal expansion/contraction corresponding to the release/adsorption of crystal water are irreversible.

In order to further demonstrate the process of releasing crystal water at different temperature, the temperature dependent XRD and Raman spectra, and the DSC/TG were performed. Fig. 5 shows the temperature dependent XRD patterns (a) and DSC/TG curves (b) of $Y_2Mo_3O_{12}$. At RT, $Y_2Mo_3O_{12}$ crystallizes in orthorhombic structure with fewer diffraction peaks due to heavy hygroscopicity[23,24]. From RT to 393 K, the diffraction peaks become sharper and more intense with increasing temperature but no additional diffraction peaks appear. Above 393 K, additional diffraction peaks according to orthorhombic $Y_2Mo_3O_{12}$ appear and become much sharper and more intense till 413 K. Fig. 5b shows the DSC (-☆-) and TG (-■-) curves of the sample in the corresponding temperature range. Both endothermic and weight loss processes show two stages corresponding to different types of crystal water release. The temperature 393 K is the turn point of the two processes and the temperature 413 K is near the complete release of crystal water. Therefore, the distinct change in XRD between 393 and 413 K indicates a notable change in the lattice of $Y_2Mo_3O_{12}$. Below 393 K, the water species released are weakly interacted with the lattice of $Y_2Mo_3O_{12}$. Above 393 K the water species interacting strongly with the lattice of $Y_2Mo_3O_{12}$ start to release.

Fig. 5c shows the temperature-dependent Raman spectra of $Y_2Mo_3O_{12}$ from 200 to 1100 cm^{-1}. The Raman modes between 900-1050 and 750-900 cm^{-1} can be

identified as internal symmetric stretching and asymmetric stretching of the MoO_4 tetrahedra and 300-400 cm^{-1} as bending vibrations of the MoO_4 tetrahedra and YO_6 octahedra.[16,17] From RT to 373 K, the Raman spectra remain nearly unchanged, indicating the release of physically adsorbed water species. However, above 373 K, there is an obvious blue shift of the symmetric stretching mode and splitting of the asymmetric stretching modes. Between 408 and 413 K, a distinct change of the Raman spectra occurs. These changes correspond to the release of crystal water chemically bonded (hydrogen bonding) in the microchannels and the crystal water is nearly complete depleted around 413 K. In order to see the release of crystal water, we show in Fig. 5d the Raman spectra in the bending vibrational region of crystal water around 1616 cm^{-1}.[25] It shows clearly that the counts of the crystal water decreases with increasing temperature and depletes around 413 K.

3.4 Crystal structure change during releasing crystal water

The crystal structure at RT corresponds to a fully hydrated form of $Y_2Mo_3O_{12} \cdot 3H_2O$ with space group *Pba2* while it transforms to *Pbcn* after complete depletion of crystal water. There is structure evolution during crystal water releasing. The AFM images and surface profiles recorded in Fig.2-4 at different temperatures correspond to surface morphology evolutions, not the crystal structure change caused by crystal water releasing because it is not possible to record the lattice points by AFM. Nevertheless, the evolution of high resolution AFM images may reflect the changing effect of several unit cells of $Y_2Mo_3O_{12}$ crystal as a whole. Both theoretical experimental studies reveal that crystal water is bonded to Y^{3+} with its O and each of the hydrogen atoms of H_2O is hydrogen bonded to the next nearest bridging O.[22,24] The formation of crystal water serves as a spring to drag the polyhedrons YO_6 and MoO_4 closer and leads to a reduced angle of Y-O-Mo and shortened Y-Mo distance.

Consequently, the volume contraction is almost linearly to the increasing number of water molecules per unit cell.[22] On the other hand, the releasing of crystal water on heating will lead to an expansion of crystal volume. Between 373 and 393 K, the crystal experiences an expansion and contraction due to crystal water releasing.

4. Conclusions

The surface morphology evolution of $Y_2Mo_3O_{12}$ ceramics with releasing of crystal water has been pursued by AFM. It is found that both the shape and size of individual grains and the integration morphology of sample exhibit dynamic changes with increasing temperature. Some grains at the valley grow up while those at higher brae and top contract obviously becomes more flaten accompanied by a grain size incease till about 373 K; the surface of the grains become obviusly wrinkled with further increasing temperature till about 393 K and the wrinkles disappear at 413 K. The evolution of the surface morphology of the sample are closely correlated with the forces induced by lattice contracting and expanding of the samples during crystal water releasing. The results also suggest that AFM can be used as a powerful tool to pursue microstructure/morphology evolution of NTE materials during giant contraction or expansion.

References

1 T. A. Mary, J. S. O. Evans, T. Vogt and A. W. Sleight, *Science*, 1996, **272**, 90-92.

2 C. A. Kennedy, M. A. White and A. P. Wilkinson, T. Varga, *App. Phys. Lett.*, 2007, **90**, 151906.

3 A. L. Goodwin, M. Calleja, M. J. Conterio, M. T. Dove, J. S. O. Evans, D. A. Keen, L. Perters and M. G. Tucker, *Science*, 2008, **319**, 794-797.

4 C. W. Li, X. L. Tang, J. A. Munoz, J. B. Keith, S. J. Tracy, D. L. Abernathy and B. Fultz, *Phys. Rev. Lett.*, 2011, **107**, 195504.

5 J. Chen, L. L. Fan, Y. Ren, Z. Pan, J. X. Deng, R. B. Yu and X. R. Xing, *Phys. Rev. Lett.*, 2013, **110**, 115901.

6 M. M. Wu, C. Wang, Y. Sun, L. H. Chu, J. Yan, D. F. Chen, Q. Z. Huang and J. W. Lynn, *J. Appl. Phys.*, 2013, **114**, 123902.

7 J. S. O. Evans, T. A. Mary and A. W. Sleight, *J. Solid State Chem.*, 1998, **137**, 148-160.

8 M. M. Wu, J. Peng, S. B. Han, Z. B. Hu, Y. T. Liu and D. F. Chen, *Ceram. Int.*, 2012, **38**, 6525-6529.

9 E. J. Liang, *Rec. Pat. Mater. Sci.*, 2010, **3**, 106-128.

10 K. Kamali, T. R. Ravindran, C. Ravi, Y. Sorb, N. Subramanian and A. K. Arora, *Phys. Rev. B*, 2012, **86**, 144301.

11 N. Khosrovani, A. W. Sleight and T. Vogt, *J. Solid State Chem.*, 1997, **132**, 355-360.

12 R. Benaventea, A. Borrella, M. D. Salvadora, O. Garcia-Morenob, F. L. Peñaranda-Foixc and J. M. Catala-Civerac, *Ceram. Int.*, 2014, **40**, 935-941.

13 J. Yan, Y. Sun, C. Wang, L. Chu, Z. Shi, S. Deng, K. Shi and H. Lu, *Scripta. Mater.*, 2014, **84-85**, 19-22.

14 Y. W. Long, N. Hayashi, T. Saito, M. Azuma, S. Muranaka and Y. Shimakawa, *Nature*, 2009, **458**, 60-64.

15 M. Azuma, W. Chen, H. Seki, M. Czapski, S. Olga, K. Oka, M. Mizumaki, T. Watanuki, N. Ishimatsu, N. Kawamura, S. Ishiwata, M. G. Tucker, Y. Shimakawa and J. P. Attfield, *Nat. Commun.*, 2011, **2**, 347.

16 E. J. Liang, H. L. Huo, J. P. Wang and M. J. Chao, *J. Phys. Chem. C*, 2008, **112**, 6577-6581.

17 Z. Y. Li, W. B. Song and E. J. Liang, *J. Phys. Chem. C*, 2011, **115**, 17806-17811.

18 B. A. Marinkovic, M. Ari, R. R. de Avillez, F, Rizzo, F. F. Ferreira, K. J. Miller, M. B. Johnson and M. A. White, *Chem. Mater.*, 2009, **21**, 2886-2894.

19 S. Sumithra and A. M. Umarji, *Mater. Res. Bull.*, 2005, **40**, 167-176.

20 S. D. Gates, *PhD Dissertation*, University of Toledo, 2008, 134-142.

21 H. F. Liu, X. C. Wang, Z. P. Zhang and X. B. Chen, *Ceram. Int.*, 2012, **38**, 6349-6352.

22 M. Y. Wu, L. Wang, Y. Jia, Z.X. Guo and Q. Sun, *AIP Advance*, 2015, **5**, 027126-9.

23 S. D. Gates and C. Lind, *J. Solid State Chem.*, 2007, **180**, 3510-3514.

24 X. S. Liu, Y. G. Cheng, E. J. Liang and M. J. Chao, *Phys. Chem. Chem. Phys.*, 2014, **16**, 12848-12857.

25 W. Y. Jia, E. Strauss, W. M. Yen, K. H. Xia and M. G. Zhao, *Phys. Rev. B*, 1989, **39**, 12853-12860.

Figure captions

Fig. 1 Crystal morphology and lattice diffraction. TEM image (insert: diffraction pattern) (a) and lattice diffraction fringes (b) of $Y_2Mo_3O_{12}$: nano-scale grains of $Y_2Mo_3O_{12}$ appear to reunite into larger one; no lattice distortion is observed from the regular lattice diffraction fringes.

Fig. 2 3D AFM images of crystal surface. 3D images of $Y_2Mo_3O_{12}$ bulk ceramics with increasing temperature from 293 to 413 K.

Fig. 3 Slices and area of AFM images and thermal expansion. (a) *XOZ* plane, (b) *YOZ* plane, (c) 45° between *XOZ* and *YOZ* plane; Areas change of grain profiles corresponding to the slices in different planes (*XOZ, YOZ* and 45° between *XOZ* and *YOZ* planes) cross the centers of the AFM images (Fig. 2) with increasing temperature, and (d) relative length change of $Y_2Mo_3O_{12}$ ceramic with a heating/cooling cycle. (e,f) Relative length change of $Y_2Mo_3O_{12}$ with heating/cooling cycle in air and in the vacuum with the pressure of -0.1 MPa.

Fig. 4 3D AFM images of crystal surface. 3D AFM images with 2 μm × 2 μm area of ceramic bulk $Y_2Mo_3O_{12}$ with increasing temperature from 293 to 413 K.

Fig. 5 Characterization of the release of crystal water. Temperature dependent XRD patterns (a) and DSC/TG curves (b) of $Y_2Mo_3O_{12}$. Temperature dependent Raman spectra of $Y_2Mo_3O_{12}$ (c) 200-1100 cm^{-1}, and (d) 1550-1700 cm^{-1}.
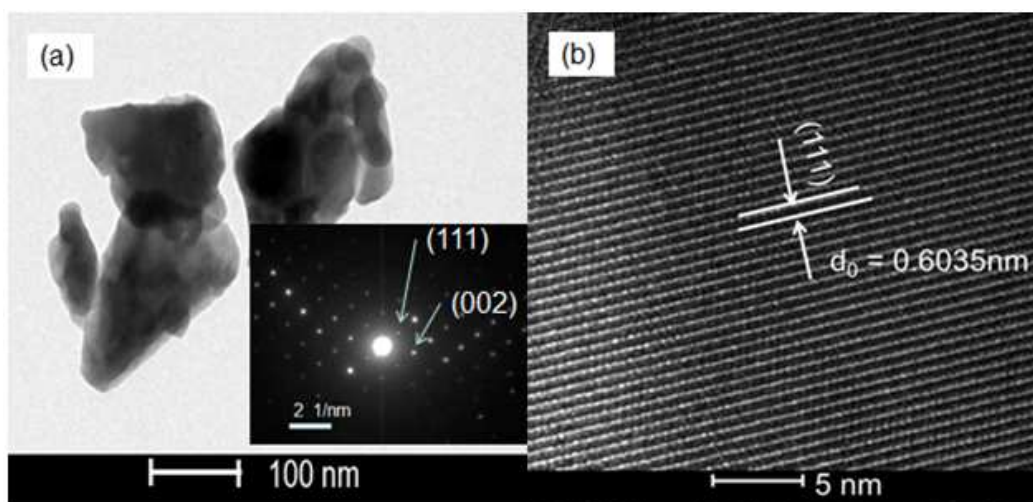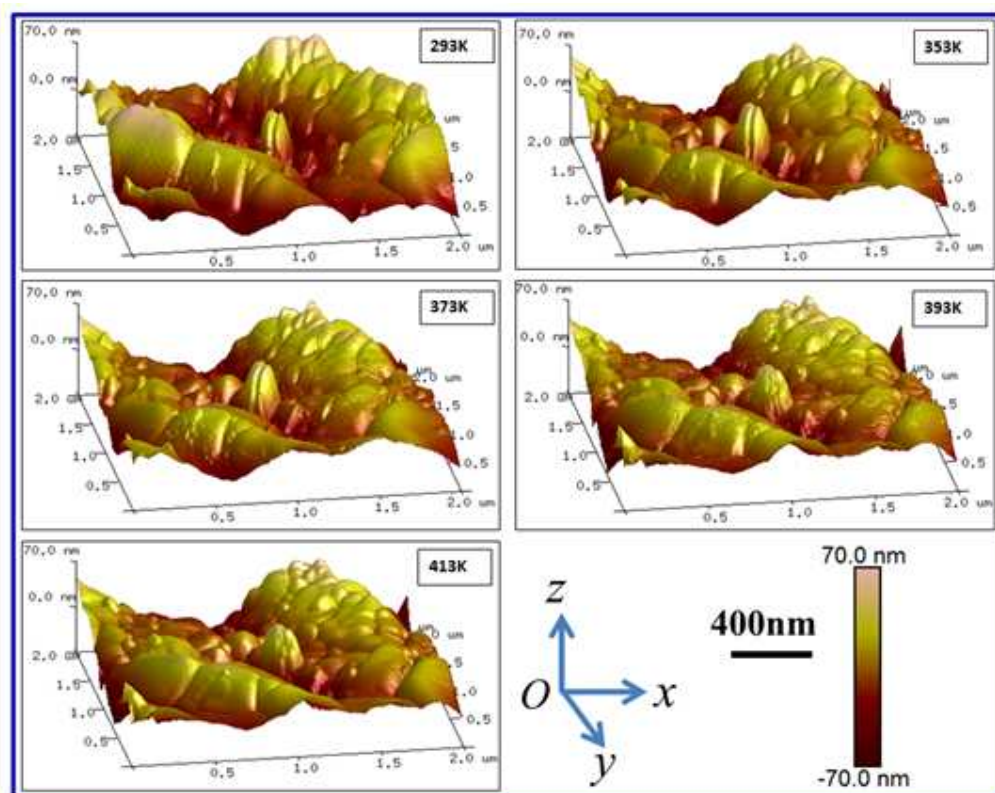
Fig. 1

Fig. 1 Crystal morphology and lattice diffraction. TEM image (insert: diffraction pattern) (a) and lattice diffraction fringes (b) of $Y_2Mo_3O_{12}$: nano-scale grains of $Y_2Mo_3O_{12}$ appear to reunite into larger one; no lattice distortion is observed from the regular lattice diffraction fringes.

Fig. 2

Fig. 2 3D AFM images of crystal surface. 3D images of $Y_2Mo_3O_{12}$ bulk ceramics with increasing temperature from 293 to 413 K.
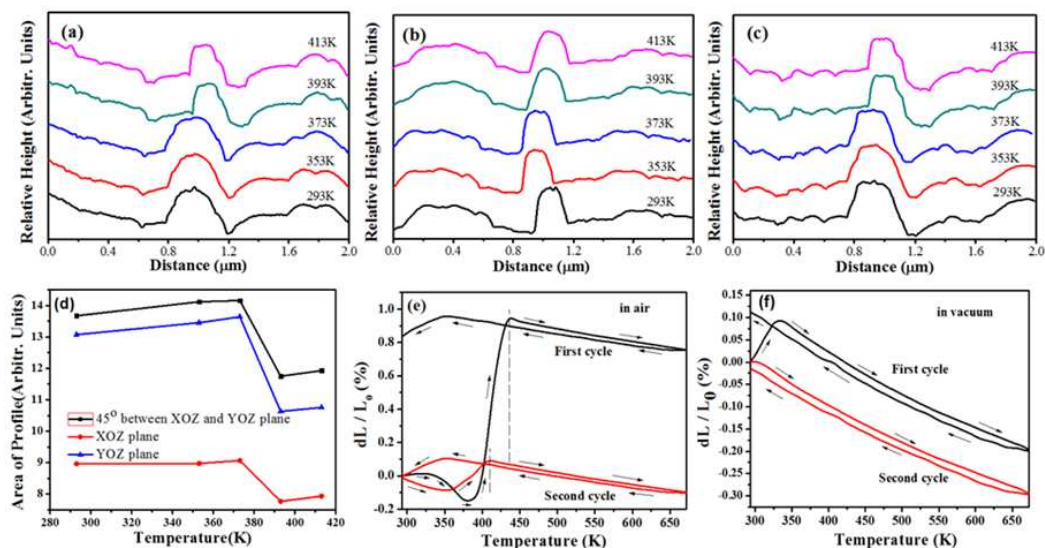
Fig. 3

Fig. 3 Slices and area of AFM images and thermal expansion. (a) *XOZ* plane, (b) *YOZ* plane, (c) 45° between *XOZ* and *YOZ* plane; Areas change of grain profiles corresponding to the slices in different planes (*XOZ*, *YOZ* and 45° between *XOZ* and *YOZ* planes) cross the centers of the AFM images (Fig. 2) with increasing temperature, and (d) relative length change of $Y_2Mo_3O_{12}$ ceramic with a heating/cooling cycle. (e,f) Relative length change of $Y_2Mo_3O_{12}$ with heating/cooling cycle in air and in the vacuum with the pressure of -0.1 MPa.
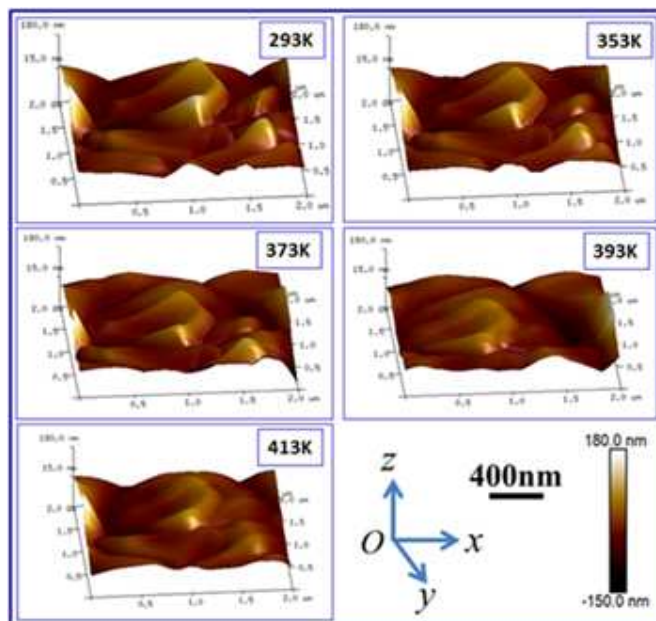
Fig. 4

Fig. 4 3D AFM images of crystal surface. 3D AFM images with 2 μm × 2 μm area of ceramic bulk $Y_2Mo_3O_{12}$ with increasing temperature from 293 to 413 K.
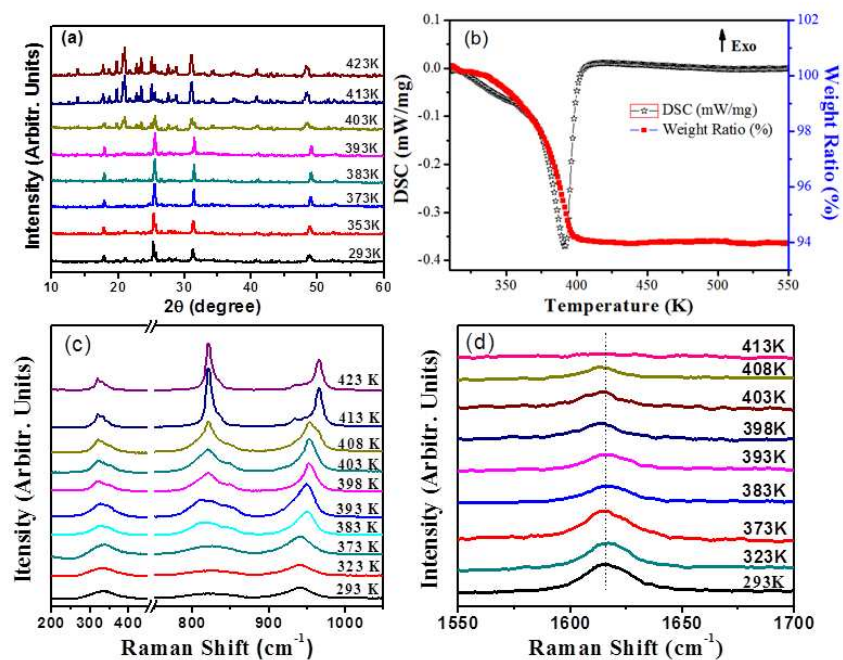
Fig. 5

Fig. 5 Characterization of the release of crystal water. Temperature dependent XRD patterns (a) and DSC/TG curves (b) of $Y_2Mo_3O_{12}$. Temperature dependent Raman spectra of $Y_2Mo_3O_{12}$ (c) 200-1100 cm^{-1}, and (d) 1550-1700 cm^{-1}.